Contents

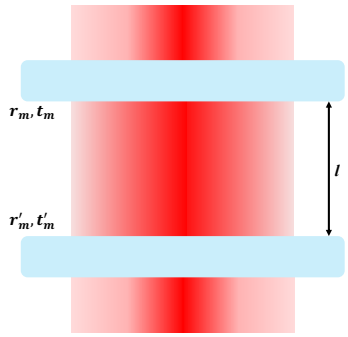

(a) Broadband cavity.

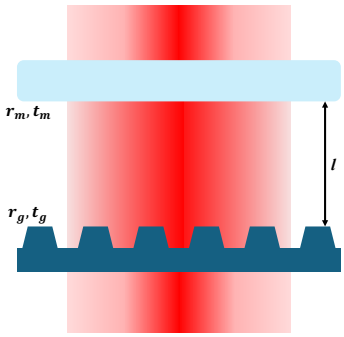

(b) Single Fano cavity.

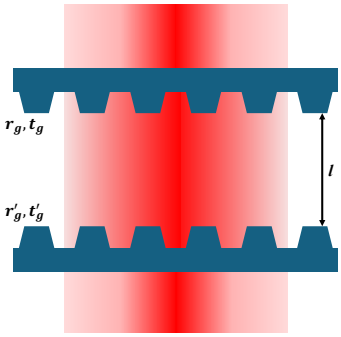

(c) Double Fano cavity.

1 Introduction

2 Theory

2.1 The Fabry-Perot interferometer

The Fabry-Perot interferometer, also known as an optical cavity, is generally comprised of two reflective optical resonators. It might make use of the configuration sketched in figure 2.

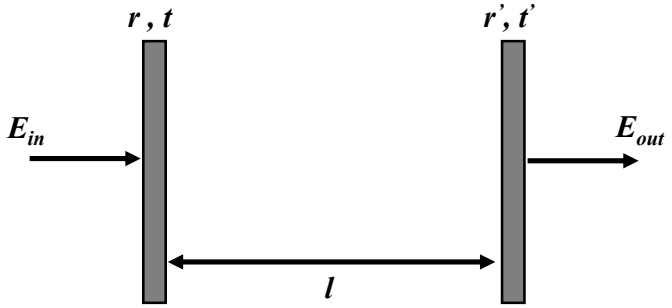

Figure 2: Sketch of a planar Fabry-Perot cavity.

Two planar slabs described by each their respective reflectivity r and transmission t are placed parallel and at a distance l from eachother. The transmitted field E_{out} is then given as a super position of all beams coupling into the cavity by E_{in}. In this way the Fabry-Perot cavity gives rise to so-called eigenstates[1] related to it's length l, derived from considering the path difference between succesive parallel beams throught the cavity. The allowed modes inside the cavity are generally limited to ones which fulfill the identity[2]

$$2l\cos\theta = m\lambda. \tag{1}$$

Here θ is the incidence angle of the light coupling into the cavity, λ is the wavelength of the light and $m = 1, 2, 3, ...$ is a positive integer describing the order of the allowed mode. For the rest of this thesis it will be assumed that the laser couples into the cavity at normal incidence, meaning that $\theta = 0^\circ$ and thus $\cos\theta = 1$, as depicted in figure 2.

2.1.1 Transmission

In order to determine the transmission throught the Fabry-Perot interferometer, we once again consider the configuration in figure 2. It is further,

initially, assumed that resonators are both lossless, such that

$$|r|^2 + |t|^2 = |r'|^2 + |t'|^2 = 1. \tag{2}$$

This means that all losses, e.g. absorption, associated with the interaction between the field and the resonators are neglected.

In order to formulate the transmitted field E_{out} in terms of the ingoing one E_{in}, we first assume that the ingoing field can be described well by a plane-wave propagating in the z-direction

$$E_{in} = E_{0,in} e^{ikz}, \tag{3}$$

where $k = 2\pi/\lambda$ is the wave number and $E_{0,in}$ is the amplitude of the field. We then consider E_{out} to be comprised of contributions for each roundtrip inside the cavity. This can be written as an infinite geometrical series given as

$$\begin{aligned} E_{out} &= tt' E_{0,in} e^{ikz} + tt' E_{0,in} e^{ikz} rr' e^{i\delta} \\ &\quad + tt' E_{0,in} e^{ikz} \left(rr' e^{i\delta}\right)^2 + tt' E_{0,in} e^{ikz} \left(rr' e^{i\delta}\right)^3 + ... \\ &= tt' E_{0,in} e^{ikz} \sum_{m=0}^{\infty} \left(rr' e^{i\delta}\right)^m \end{aligned} \tag{4}$$

where $\delta = 2kl$. The first term of the series corresponds to a direct transmission through the cavity, and each term thereafter corresponds to the respective contribution to the transmission after the $m'th$ round trip.

By evaluating the series it is seen that it indeed converges, and setting $z = l$ the final expression for the transmission through a planar Fabry-Perot cavity is found as

$$E_{out} = E_{0,in} \frac{tt' e^{i\delta/2}}{1 - rr' e^{i\delta}}. \tag{5}$$

Figure 3 shows an example of the normalized transmission $|E_{out}|^2/|E_{0,in}|^2$ of an arbitrary Fabry-Perot cavity of length $l \approx 50\mu m$ with reflectivity

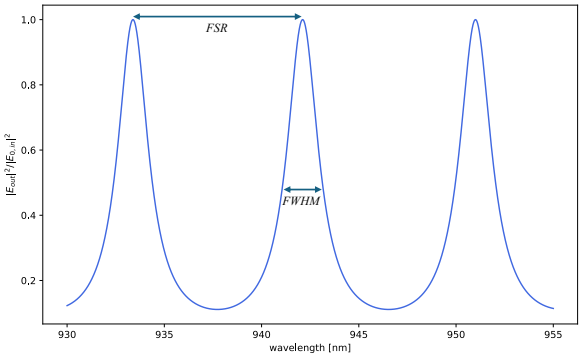

Figure 3: Example of a Fabry-Perot cavity transmission (50um cavity length and $|r|^2 = 0.5$)

$|r|^2 = 0.5$. The two defining features marked on the figure are the *Free Spectral Range (FSR)* and *Full Width at Half Maximum (FWHM)*. As clearly depicted on the figure, the FSR is defined as the, in this case, spectral distance between two peaks in the spectra[1], while the FWHM is simply the linewidth of each peak.

2.1.2 Finesse

Another important characteristic of an optical cavity is the so-called *finesse* $\mathcal{F}$, which generally describes the quality of the cavity by the number of round trips the light makes on average before being transmitted. It can thus be said that the finesse corresponds to the order m in the geometrical series describing the transmitted field E_{out} in eq. (4), making the series, in any practical sense, finite.

There is a variety of ways one can obtain the finesse of a cavity. By examination of the spectrum one can find the finesse in terms of the FSR and FWHM, as seen in figure 3, given as

$$\mathcal{F} = \frac{FSR}{FWHM}, \tag{6}$$

which indicates the resulting peaks of a cavity of higher finesse are narrower for the same FSR.

[1]The definition of the FSR is not limited to the distance between peaks in wavelength. As seen in eq. (1) the cavity length and the resonant wavelengths are linearly dependent, and the length can thus just as well be varied resulting in a similar spectrum for the cavity transmission.

The finesse can also be expressed in terms of the reflectivity/transmission of the resonators of the cavity, as the defining phyisical action is that of the light either being transmittied from the cavity or not. The finesse in terms of r and t, for both resonators, are given as

$$\mathcal{F} = \frac{2\pi}{1 - |r|^2 + 1 - |r'|^2} = \frac{2\pi}{|t|^2 + |t'|^2}. \tag{7}$$

Figure 4 shows an example of the transmission spectrum of a high finesse cavity of reflectivity $|r|^2 = 0.9$ together with a low finesse cavity of reflectivity $|r|^2 = 0.3$. It is clearly seen that the linewidth of the high finesse cavity is much narrower than the low finesse case, which follows the relation shown in eq. (6).

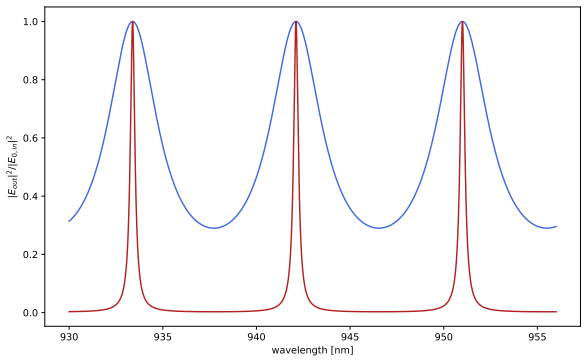

Figure 4: Comparison of an arbitrary Fabry-Perot cavity of high and low finesse, respectively. The high finesse cavity and a reflectivity of $|r|^2 = 0.90$, while for the low finesse cavity $|r|^2 = 0.30$.

Eq. (7) however is only true for the case of a lossless cavity, i.e. when eq. (2) is fulfilled. In practice, any cavity will have some amount of losses, which would have to be taken into account when calculating the finesse. When losses are present eq. (2) instead generally reads

$$|r|^2 + |t|^2 + L + L' = 1, \tag{8}$$

where L and L' indicates the fractional losses of each resonator.

In this case the finesse would be given as

$$\mathcal{F} = \frac{2\pi}{1 - |r|^2 + 1 - |r'|^2} = \frac{2\pi}{|t|^2 + |t'|^2 + L_{total}}. \tag{9}$$

The effect on the transmission spectrum of a cavity with losses is that the level of the normalized transmission will not reach 1, as some light is lost to i.g. absorption effects for each round trip of the cavity.

2.1.3 Cavity length

So far we have only considered effects that are independent of the length of the Fabry-Perot cavity, and by examining figure 4 it is seen that the only previously discussed feature that does not vary when changing the reflectivity and transmission (and by extension also the finesse) of the cavity, is the FSR. The FSR is defined as the distance between adjacent peaks of the transmission spectrum, and is given as

$$FSR = \frac{c}{2nl}, \tag{10}$$

where c is the speed of light in vacuum, n is the refractive index of the medium inside the cavity and l is the length of the cavity. The inverse proportionality of the cavity length l and the FSR is easily seen, and since the finesse is constant when varying the cavity length, the same must apply for the FWHM. Figure 5 shows a comparison of the transmission through two Fabry-Perot cavities of length $100\mu m$ and $150\mu m$, respectively. It is evident that the FSR depends on the cavity length, as $FSR_{100\mu m} > FSR_{150\mu m}$. It is also seen, that while the FSR becomes smaller with increasing cavity lengths, the linewidth does too, this is a consequence of the finesse $\mathcal{F}$ being constant in terms of the cavity length.

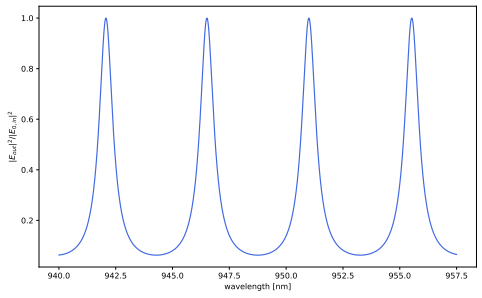

(a) $\sim 100\mu m$ Fabry-Perot cavity transmission.

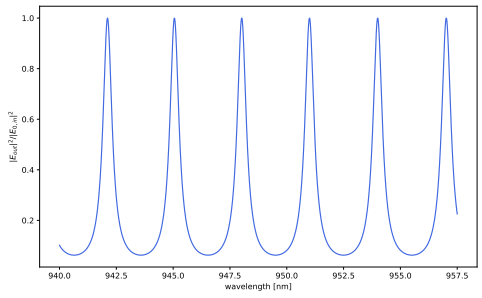

(b) $\sim 150\mu m$ Fabry-Perot cavity transmission.

Figure 5

2.1.4 The Fundamental Mode: A Gaussian Beam in the Large Waist Approximation

In order to describe the allowed modes within an optical cavity, it is first assumed that a single-mode field is linearly polarized. We then consider solutions to the wave equation

$$\nabla^2 \vec{E} = \frac{1}{c^2} \frac{\partial^2 \vec{E}}{\partial t^2}, \tag{11}$$

given as

$$\vec{E} = E_0(x, y, z)\vec{\epsilon} e^{ikz}. \tag{12}$$

Here $E_0(x, y, z)$ describes the electric field amplitude, $\vec{\epsilon}$ is denoted the polarization vector and $k = 2\pi/\lambda$ is the angular wave number of the field propagating along the z-axis. It is assumed that the electric field has a Gaussian transverse distribution[2].

This is almost the simplest description of the propagating field, however, as the spacial dependence of the field amplitude still might cause problems, we consider the range in which this can be neglected.

It can be shown from the derivation of the Gaussian distribution that the waist of the beam $w(z)$, which depends on the spacial coordinate in the direction of propagation, can be described as [1]

$$w(z) = w_0 \sqrt{1 + \left(\frac{z}{z_R}\right)^2}, \tag{13}$$

where z is the distance from focus, w_0 is the beam waist at focus and z_R is the so-called *Rayleigh range*. The Rayleigh range describes the range in which the beam diverges slowly, whereas after this has been surpassed, the beam will begin to diverge more rapidly. By quick inspection of eq. (13) it is seen that

$$w(z) = \begin{cases} w_0, & \text{for } z = 0 \\ w_0\sqrt{2}, & \text{for } z = z_R, \end{cases} \tag{14}$$

[2]When this is the case, the laser is said to operate in the lowest possible mode denoted TEM_{00}. This implies the assumption of ideal lasing conditions.

which shows that the beam waist diverges no more than by a factor of $\sqrt{2}$ from the optimal case, for $0 \leq z \leq z_R$. Considering the case where $z \neq 0$ but however much smaller than the Rayleigh range z_R, we can further inspect eq. (13) and find that this leads to negligible changes in the waist of the beam. Specifically, it can fairly easily be seen that

$$\left(\frac{z}{z_R}\right)^2 \approx 0, \quad \text{for } z << z_R \tag{15}$$

which in turn leads to

$$w(z) \approx w_0. \tag{16}$$

The Rayleigh range can be written as [2]

$$z_R = \frac{\pi w_0^2}{\lambda}, \tag{17}$$

which, through the exponential dependence on w_0, shows that a large beam waist will result in a long Rayleigh range. As an example, consider a beam of waist $w_0 = 200\mu m$ and wavelength $\lambda = 950nm$. This would result in a Rayleigh range of $z_R = 13.23cm$.

Finally we can conclude, that any optical cavity, for which the total distance travelled inside the cavity[3], is significantly shorter than the Rayleigh range of the incident beam, the spacial dependence of the field amplitude inside the cavity is negligible, and the fundamental mode can be described simply by a linearly polarized plane wave

$$\vec{E} = E_0 \vec{\epsilon} e^{ikz}. \tag{18}$$

This is often referred to as the *large waist approximation* of a Gaussian beam, due to the dependence on w_0 of eq. (17).

[3]For any optical cavity the incident light will travel a distance inside the cavity according to, not only the length of the cavity, but also the amount of round trips the light makes when confined inside the cavity.

2.2 The Fano mirror: a sub wavelength grating

2.2.1 Geometric optical analysis

Considering an ideal grating with period d in the sub-wavelength regime, it can be shown that only a single mode of reflection/transmission is supported.

Any grating, of arbitrary dimensions, must comply with the very general *grating equation*[2] given as

$$\sin\theta_m = m\frac{\lambda}{d}, \tag{19}$$

for the special case of a linearly polarized plane wave incident on a grating placed normal to the direction of propagation. Now, inserting the sub-wavelength condition $d \ll \lambda$, it is easily seen that the right side of the equation blows up for any order of reflection $|m| > 0$, effectively showing that this is the aforementioned single supported mode in this regime. Furthermore, it can be equally easily seen that the propagation direction of the 0'th order mode is the same as the incident beam, i.e. normal to the grating.

2.2.2 Reflection/transmission spectra and line shape analysis

2.2.3 Lossless grating

We wish to analytically describe the wavelength-dependent spectra for the transmission and reflectivity of an infinite sub-wavelength grating. By first considering the case where absorption and thermal coupling effects are neglected, i.e. a lossless grating, we can assume conservation of energy and thereby the relations

$$|r_g|^2 + |t_g|^2 = 1 \quad \text{and} \quad |r_d|^2 + |t_d|^2 = 1, \tag{20}$$

where the subscripts g and d indicate the *grating* and *direct* transmissions and reflectivities, respectively. It is implied that the direct coefficients are constants and describe the transmission and reflectivity when the incident wavelength is significantly detuned from any guided-mode resonance of

the grating. Furthermore, it is also implied that the grating coefficients are functions of the incident wavelength.

We now assume a normal incident beam on the grating as a linearly polarized monochromatic plane wave, with a wavelength close to a guided-mode resonance of the grating. In order to describe the coefficients r_g and t_g we follow the formalism presented by Fan and Joannopoulos [3] and consider the likely paths of the incident light through the grating. It is quite intuitive to consider the case where the light is simply transmitted, and this shall be our first case hereafter denoted the *direct pathway*. Another case one might consider is the one where the incident light excites the guided-mode resonance in the grating. This case is denoted the *indirect pathway* and decays more slowly than it's direct counterpart.

The interference caused when the guided mode is excited is often referred to as *Fano resonances*, due to its physical similarities to the description of interference between a discrete autoionized state and a bound continuum state first reported by Fano [4]. The cross section of inelastic scattering, when measured as a function of energy, showed characteristic asymmetric peaks. These were described as the aforementioned interference pattern between *direct* (the discrete state) and *indirect* (the continuum state) pathways.

By generalizing the model of Fan and Joannopoulos [3] we describe the transmission and recletivity coefficent amplitudes as

$$r_g = r_d + \frac{a}{k - k_1 + i\gamma} \quad \text{and} \quad t_g = t_d + \frac{b}{k - k_1 + i\gamma}, \tag{21}$$

where $k = 2\pi/\lambda$ is the incident wave number, $k_1 = 2\pi/\lambda_1$ is the wave number according to the guided-mode resonance and γ is the HWHM (half width at half maximum) of the guided-mode resonance. Complex coefficients a and b describe the interference between the directly transmitted or reflected waves and the guided mode of the grating.

Note that in eq. (21) the right side of the expression for each coefficient corresponds to the continuum state i.e. the indirect pathway, while the direct transmission and reflection coefficients take the role of the

autoionized discrete state, i.e. the direct pathway[4] [4]

As we are dealing with an ideal, lossless, grating, we assume coefficients a and b to be equal, meaning that we specifically assume vertical symmetry throughout the grating. By considering eq. (20) this in turn leads to

$$a = b = -i\gamma(t_d + r_d), \tag{22}$$

which further yields an expression for the grating transmission amplitude coefficient on the form

$$t_g = t_d \frac{k - k_0}{k - k_1 + i\gamma}. \tag{23}$$

Here, the newly introduced $k_0 = 2\pi/\lambda_0$ is the zero-transmission/unity-reflectivity wave number.

To generalize eq. (23) to include non-unity reflectivity and non-zero transmission, we allow for $a \neq b$ meaning that the case of vertical asymmetry is included in the model. By assuming $r_d, t_d \in \mathbb{R}$, eq. (20) leads to the coupled differential equations

$$\begin{aligned} &t_d x_a + r_d x_b = 0, \quad \text{and} \\ &x_a^2 + y_a^2 + x_b^2 + y_b^2 + 2t_d\gamma y_a + 2r_d\gamma y_b = 0, \end{aligned} \tag{24}$$

where $\{x, y\}_{a,b}$ respectively denotes the real and imaginary parts of the coefficients a and b. Solving eqs. (24) leads to the correct complex reflectivity coefficients and the expression for the transmission coefficient amplitudes now reads

$$t_g = t_d \frac{k - k_0 + i\beta}{k - k_1 + i\gamma}, \tag{25}$$

where k_0 and β are defined from the expression for a found by solving eqs. (24), given as

$$a = t_d(k_1 - k_0 - i\gamma + i\beta). \tag{26}$$

Finally, this allows for non-zero transmission and non-unity reflectivity at wave number k_0.

[4]The general eigenvector of a state comprised of a super-position between a discrete state and a continuum, i.e. a state vector corresponding to a Fano resonance, is given as $\Psi_E = a\phi + \int dE' b_{E'}\psi_{E'}$, given in eq. (2) in ref. [4], where a and $b_{E'}$ describes the probability of either pathway.

2.2.4 Lossy grating

In order to modify the above model such that losses, e.g. due to absorption or thermal coupling effects, are accounted for, we add a resonant loss term to the energy conservation relation in eq. (20). For this we introduce the resonant loss level L, which must be known in order to accurately calculate the complex reflectivity coefficients. The energy conservation relation is modified such that

$$|t_g|^2 + |r_g|^2 + \frac{c^2}{(k-k_1)^2+\gamma^2} = 1, \tag{27}$$

where the coefficient $c^2 = L((k-k_1)^2+\gamma^2)$ includes the resonant loss term L. A new set of coupled differential equations are found, using eq. (27), given as

$$\begin{aligned} &t_d x_a + r_d x_b = 0, \quad \text{and} \\ &x_a^2 + y_a^2 + x_b^2 + y_b^2 + c^2 + 2t_d\gamma y_a + 2r_d\gamma y_b = 0. \end{aligned} \tag{28}$$

It is easily identified that eq. (24) and eq. (28) differ only by the addition of coefficient c^2, and thereby the losses. Solving eq. (28) leads to the correct complex reflectivity coefficients, except that they now account for any losses associated with the grating.

In conclusion, the complete grating model consists of an expression for the transmission coefficients and a set of coupled differential equations for the reflection coefficients, shown in eq. (25) and eq. (28), respectively. The model on the form used for this project and subsequent thesis is derived in previous work by A. Darki et al. [5] and more recently T. Mitra et al. [6].

2.3 The Fano cavity

2.3.1 The single Fano cavity model

The single Fano cavity consists of a planer broadband mirror, and a sub-wavelength grating, i.e. a Fano mirror, as described in section 2.2 and seen in figure 6 where schematics of the single Fano and broadband cavity configurations are shown. While the broadband mirror has fixed optical properties, the Fano mirror has transmission and reflection coefficients dependent on the incident wavelength, according to solutions to the doupled differential equations of eq. (28).

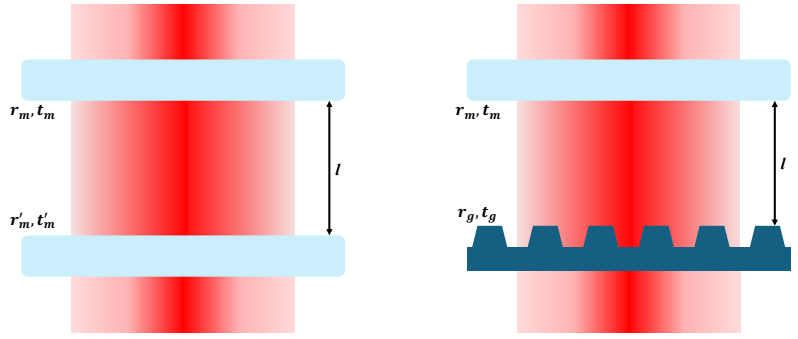

(a) Schematics of the broadband cavity.

(b) Schematics of the single Fano cavity.

Figure 6

In order to model the single Fano cavity transmission spectra, we therefore consider the transmission function of a normal incident and planer Fabry-Perot cavity in eq. (5) with $r, t \to r_m, t_m$ and $r', t' \to r_g(\lambda), t_g(\lambda)$. Here the subscript m indicates the broadband *mirror* coefficients, and g is for *grating*, which indicates the coefficients of the Fano mirror. Rewriting eq. (5) such that it describes the normalized transmission amplitude, through the single Fano cavity, $T_{cav} = |E_{out}|^2/|E_{0,in}|^2$ we get

$$T_{cav} = \left| \frac{t_m t_g(\lambda) e^{i\phi}}{1 - r_m r_g e^{2i\phi}} \right|^2, \tag{29}$$

where $\phi = 2\delta = kl$, $k = 2\pi/\lambda$ and l is the cavity length, as is consistent the general case described in section 2.2.

2.3.2 Transmission linewidth

In order to analytically describe how the transmission spectrum at, or close to, overall resonance[5] behaves as a function of the incident wavelength, we attempt to generalize the Fano model for this specific regime. Considering the case where the cavity resonance closely resembles the guided-mode resonance of the Fano mirror (the zero-transmission wavelength), eq. (29) can be approximated well by

$$T_{cav} \approx \frac{A}{1 + \left(\frac{\Delta}{1-\nu\Delta}\right)^2}, \tag{30}$$

where $\Delta = (\lambda - \lambda_c)/\delta\lambda$ is the detuning from the cavity resonance normalized by the HWHM $\delta\lambda$, and ν is a constant describing the asymmetry of the single Fano transmission spectrum.

From eq. (30) it can be shown that the HWHM of the Fano transmission profile around the resonance wavelength $\delta\lambda$ is approximately given as

$$\delta\lambda \approx \frac{1}{\frac{1}{\delta\lambda_c} + \frac{1}{\delta\lambda_g}}, \tag{31}$$

where $\delta\lambda_c$, $\delta\lambda_g$ are the contributions to the linewidth stemming from the broadband cavity and the Fano cavity in the Fano regime, respectively. It can be shown that there are two regimes of interest when examining the linewidth of the Fano cavity transmission profile. The first of these is the standard cavity regime, where the broadband and Fano cavity produces resonance transmission peaks of comparable, if not equal, linewidths. The other is the aforementioned Fano regime where a significant reduction in linewidth is found, when comparing the Fano and broadband cavity transmission profiles. In order to detemine where the transition between the standard and the Fano cavity regimes occur, we look at the expressions for $\delta\lambda_c$ and $\delta\lambda_g$ included in eq. (31). The standard cavity linewidth is given as

$$\delta\lambda_c = \frac{\lambda_0^2}{8\pi l}(|t_g(\lambda_0)|^2 + |t_m|^2 + L), \tag{32}$$

[5]This terminology is used for the scenario where the guided-mode, cavity mode and input laser mode all meet the resonance condition $\lambda_g \approx \lambda_c \approx \lambda_l$, where g, c, l stands for grating/guided-mode, cavity and laser, respectively.

while the Fano cavity linewidth in the Fano regime is given as

$$\delta\lambda_g = \frac{\gamma\lambda}{2(1-r_d)}(|t_g(\lambda_0)|^2 + |t_m|^2 + L). \tag{33}$$

Here λ_0 is the cavity resonance wavelength, l is the cavity length, $L = 1 - |r_g(\lambda_0)|^2$ is the total losses of the cavity when on resonance, $\gamma\lambda$ is the width of the guided-mode resonance of the Fano mirror and r_d is the off-resonance, or *direct*, reflectivity of the Fano mirror.

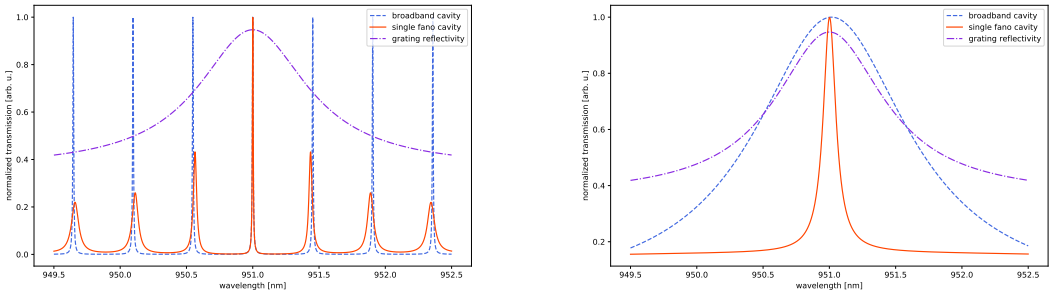

(a) Broadband and single Fano transmissions for a cavity length of $\sim 1000\mu m$, i.e. in the *standard* regime.

(b) Broadband and single Fano transmissions for a cavity length of $\sim 5\mu m$, i.e. in the *Fano* regime.

Figures 7a and 7b depicts two examples of single Fano cavity transmission spectra together with their respective complimentary broadband cavity transmission profiles, and the reflectiviy amplitude of the Fano mirror used to model both profiles. As shown in section 2.2 any Fano mirror, or grating, is described by five characterizing parameters. For the one used to model the transmission spectra in figures 7a and 7b these are

$$\begin{aligned} \lambda_0 =& 951nm, \;\; \lambda_1 = 951nm, \;\; t_d = 80\%, \\ & \gamma\lambda = 0.5nm \;\; \text{and} \;\; \beta = 10^{-6}, \end{aligned} \tag{34}$$

where we remember that $\lambda_{0,1}$ are the resonant wavelengths for, respectively, the cavity and guided-mode, t_d is the direct transmission, $\gamma\lambda$ is the width of the guided-mode resonance and β is a constant describing the losses of the grating, which here is neglected when solving the coupled differential equantions of eq. (28). The broadband mirror parameters are chosen such that it perfectly resembles the transmission and reflectivity of the grating on resonance, which is arbitrarily chosen such that $|r_m|^2 = 95\%$ and $|t_m|^2 = 5\%$.

It is clear from inspection of figure 7a that the resonance transmission profile of the standard broadband cavity is not wavelength dependent, in the sense that all fringes, when cavity losses are neglected, appear to have the same high finesse $\mathcal{F}$, i.e. ratio between the FSR and HWHM. This is not the case for the Fano cavity which is, naturally, due to the wavelength dependence of the optical properties of the Fano mirror, as this causes the transmission and reflectivity to *only* match those of the broadband mirror when on resonance.

In figure 7b, the transmission spectra of both cavities are shown *in* the Fano regime, where it is clearly seen that while the standard cavity experiences broadening for shorter cavity lengths[6], this is not the case for the Fano cavity transmission peak.

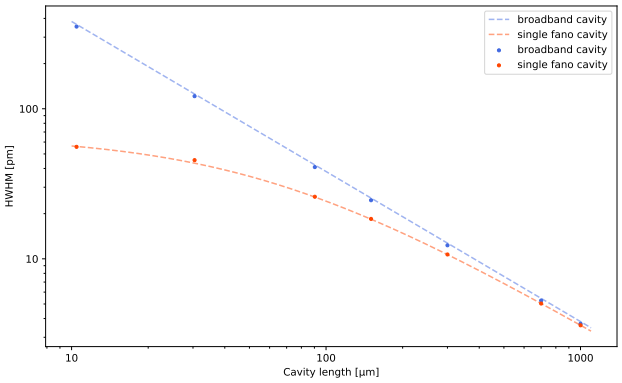

(a) The approximate analytical resonance linewidths (eq. (31)) as a function of cavity length for the broadband and single Fano cavities are shown together with linewidths of transmission profiles simulated using eq. (29) and eq. (5) for comparison.

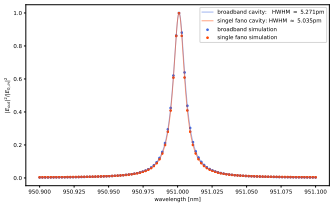

(b) Transmission spectra of broadband and single Fano cavities of length $\sim 700\mu m$.

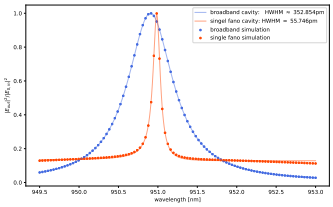

(c) Transmission spectra of broadband and single Fano cavities of length $\sim 10\mu m$.

Figure 8a models the behavior of the linewidth of the single Fano cavity compared with the one for a broadband cavity of similar optical properties, as a function of wavelength. Here it is easily seen where the linewidth of the single Fano begins to saturate, and hence deviate from the one of the broadband cavity. The plotted line in the figure is calculated using eq.

[6]This is a natural consequence of the shorter cavity as this causes the lifetime inside the cavity to fall and hense the transmission HWHM to rise. The HWHM is inversly proportional to the lifetime and goes as $\delta\lambda \propto 1/\tau$.

(31) while the points depicit linewidths found as a fitting parameter from a least squares fit of the general Fano model in eq. (30) to transmission spectra simulated by the Fabry-Perot (eq. (5)) and single Fano (eq. (29)) transmission functions. Finally, it can be concluded that the approximate analytical expression for the linewidth of the broadband and single fano cavities in eq. (31) correlates very well with the values found from the simulated spectra.

2.4 The double Fano cavity

2.4.1 The double fano transmission model

While the single Fano cavity is usually known in the appropriate litterature as simply a *Fano cavity*, I have insisted on including the fact that it contains only one Fano mirror, and hence denoted it the *single* Fano cavity. This addition is justified by the contents of this section, and namely that we now move on to the *double* Fano cavity, which as the name suggests consists of two Fano mirrors. The schematics of this configuration is shown together with the one for the single Fano cavity in figure 9.

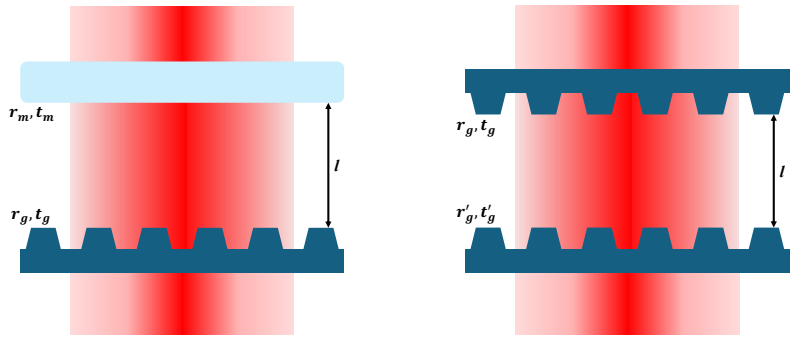

(a) Schematics of the single Fano cavity.

(b) Schematics of the double Fano cavity.

Figure 9

Here it is evident that instead of having one set of reflectivity and transmission coefficients that depend on the incident wavelength, we now have two. In order to model the transmission of the double Fano cavity, we once again consider the transmission function for the normal incident and planar Fabry-Perot cavity in eq. (5), this time with $r, t \to r_g(\lambda), t_g(\lambda)$ and $r', t' \to r'_g(\lambda), t'_g(\lambda)$. We rewrite the Fabry-Perot transmission function with the addressed substitutions of the optical coefficients and such that

it decribes the normalized transmission amplitudes $T_{cav} = |E_{out}|^2/|E_{0,in}|^2$ and get

$$T_{cav} = \frac{t_g(\lambda)t'_g(\lambda)e^{i\phi}}{1 - r_g(\lambda)r'_g(\lambda)e^{2i\phi}}. \tag{35}$$

The subscript g indicates a grating transmission or reflectivity. Figure 10 shows an example of the normalized transmission spectrum of an $\sim 30\mu m$ double Fano cavity on- and off-resonance, found using eq. (35).

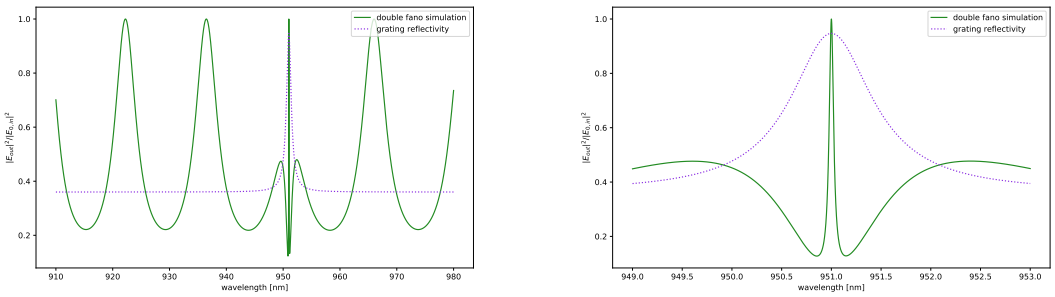

(a) (b)

Figure 10

2.4.2 Transmission linewidth

$$\delta\lambda \approx \frac{1}{\frac{1}{\delta\lambda_c} + \frac{1}{\delta\lambda_g^{double}}}, \tag{36}$$

$$\delta\lambda_c = \frac{\lambda_0^2}{8\pi l}(|t_g(\lambda_0)|^2 + |t_m|^2 + L), \tag{37}$$

$$\delta\lambda_g^{double} = \frac{\gamma\lambda}{4(1 - r_d)}(|t_g(\lambda_0)|^2 + |t_m|^2 + L). \tag{38}$$

2.4.3 Single and double Fano cavity comparison

Using the analytical expression for the double Fano cavity transmission in eq. (36) we are now in a position to compare the single and double Fano cavities. Note that we at this point only consider the ideal case of the double Fano cavity where additional cavity losses are neglected

and the two Fano mirrors used are identical, i.e. the cavity is said to be *symmetrical*. The additional cavity losses are explicitly set to be given as

$$L = 1 - |r_g|^2 - |t_g|^2 = 0. \tag{39}$$

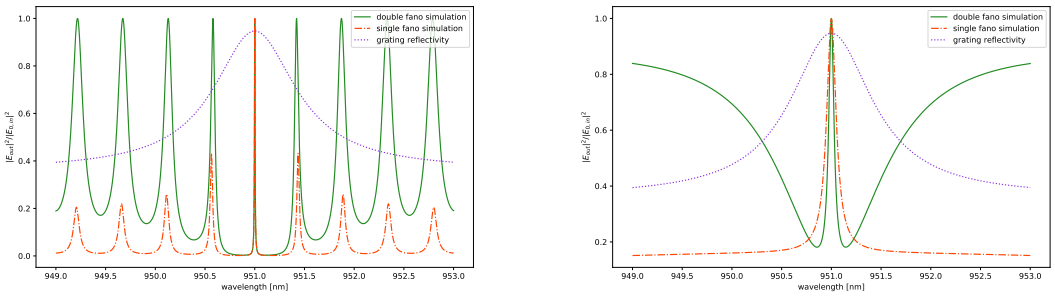

(a) (b)

Figure 11

Figure 11 shows the transmission of the ideal double Fano cavity and the corresponding single Fano cavity for comparison.

Figure 11a shows the transmission for a cavity length of $\sim 1000\mu m$ which is well-inside the standard regime outlined in section 2.3.2 where the standard broadband and single Fano cavities produce transmission spectra of almost identical linewidths. In this regime, due to the $1/l$ proportionality of the FSR, the off-resonance behavior of the double Fano cavity transmission is visible in the range plottet. It is seen, contrary to the single Fano cavity, that the transmission at each cavity resonance reaches a normalized transmission of $|E_{out}|^2/|E_{0,in}|^2 = 1$. This is due to the fact that the two gratings, while they have wavelength dependent transmission and reflectivity coefficients, always have identical ones for the ideal case which maximizes the Fabry-Perot transmission function and ensures unity transmission at any cavity resonance. The minimum level of the cavity changes according to the reflectivity of the Fano mirrors and by that the HWHM also changes as we move further from the guided-mode resonance. Both the minimum transmission level and the HWHM converge when moving away from the resonance wavelength, when the reflectivity becomes constant.

Figure 11b shows the transmission of a double Fano cavity of length $\sim 5\mu m$ which, contrary to the one in figure 11a, is well within the Fano

regime. It is seen that the double Fano cavity transmission produces a resonance peak with a HWHM narrower than the one for the single Fano cavity, as is predicted in eq. (38). Furthermore, the immediate off-resonance behavior of the double Fano cavity transmission in the Fano regime, is drastically different than for the single Fano cavity. This is due to the collective higher transmission in this region compared with the single Fano case where the broadband mirror has a constant, and often high, reflectivity and hence a correspondingly low transmission.

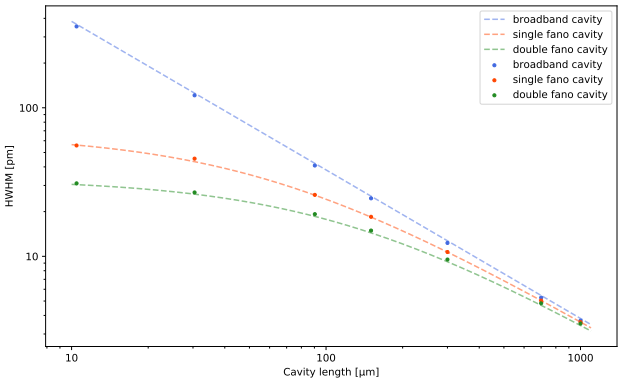

(a) The analytical resonance linewidths (eqs. (31), (36), and (32)) as a function of the cavity length for the broadband, single and double Fano cavities are shown together with linewidths of corresponding transmission profiles simulated using eqs. (29), (35), and (5) for comparison.

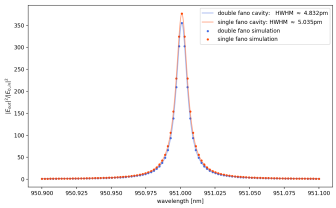

(b) Intracavity transmission spectra of single and double Fano cavities of length $\sim 700\mu m$.

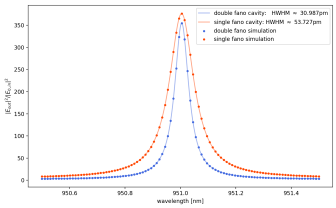

(c) Intracavity transmission spectra of single and double Fano cavities of length $\sim 10\mu m$.

Figure 12a shows the analytical linewidth calculated and compared for the broadband, single Fano, and double Fano cavities, calculated using eqs. (32), (31), (36). These are compared with linewidths found as fitting parameters from a least squares fit of the general Fano transmission formula given in eq. (30) to transmission spectra calculated using eqs. (5), (29), and (35). According to eq. (36) the linewidth of the double Fano cavity transmission should converge to exactly half that of the single Fano cavity, meaning that

$$\delta\lambda_{double} = \frac{\delta\lambda_{single}}{2}, \quad \text{for } l \to 0. \tag{40}$$

This is supported well by the simulation depicted in figure 12a.

Figures 12b and 12c contain examples of intracavity[7] spectra of single and double Fano cavities and corresponding fits to the general Fano model in order to determine their linewidths.

2.4.4 Additional cavity losses

Thus far we have only examined a lossless double Fano cavity where

$$|r_g|^2 + |t_g|^2 = 1 \tag{41}$$

is fulfilled for both Fano mirrors used to contruct the cavity.

In this section we will investigate what happens when we introduce additional cavity losses[8]

$$L = 1 - |r_g|^2 - |t_g|^2, \tag{42}$$

leading to the modified condition

$$|r_g|^2 + |t_g|^2 + L = 1. \tag{43}$$

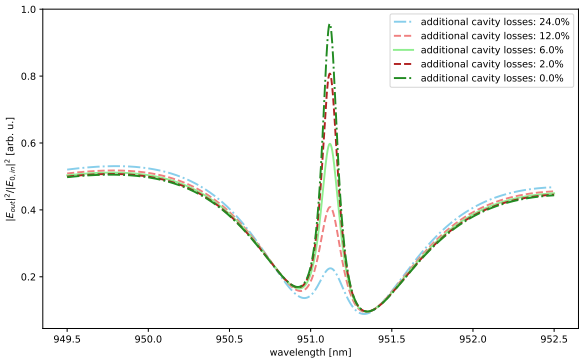

Figure 13

[7]The reason these are shown as intracavity spectra instead of transmission spectra is due to the immediate off-resonance behavior of the double Fano cavity transmission. The shape makes accurate fitting a challenge, and while the intracavity spectra cannot be measured in the lab, the linewidth when simulated is identical to the resulting transmission peaks.

[8]Not to be confused with the often used definition of cavity losses given as $L = 1 - |r|^2$ where anything not being reflected back into the cavity is considered to have a contribution to the losses.

Figure 13 shows double Fano transmisison spectra as a function of wavelength for a symmetric cavity with varying values for the additional cavity losses. It is readily seen that the maximum value reached in each spectrum is rapidly reduced with the introduction of these losses.

Since the linewidth is defined as the HWHM of the transmission profile, this will naturally vary as a function of additional cavity losses. This is depicted in figure 14a where the HWHM is shown for different values of L. Examples of intracavity spectra taken for different values of L are shown in figures 14b and 14c, along with their respective least squares fits of the general Fano model in eq. (30) and linewidths found as fitting parameters hereof.

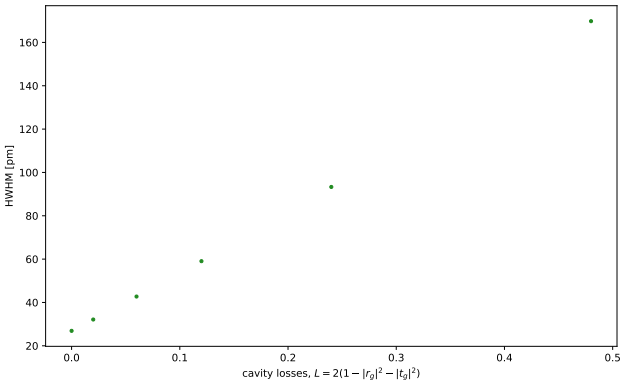

(a) HWHM of a symmetric $\sim 30\mu m$ double Fano cavity as a function of additional cavity losses $L = 2(|r_g|^2 - |t_g|^2)$. Improve this figure by adding the analytical prediction of the linewidth as a function of losses.

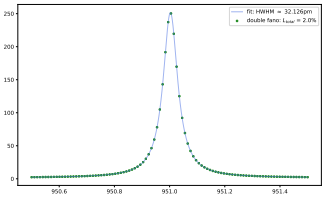

(b) Double Fano transmission spectra with cavity length $\sim 30\mu m$ and $L = 2\%$.

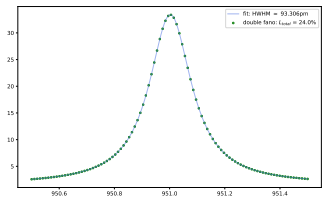

(c) Double Fano transmission spectra with cavity length $\sim 30\mu m$ and $L = 24\%$.

Figure 14

2.4.5 Spacial and spectral detuning - $l_g \geq l \geq l'_g$ & $\Delta \neq 0$ (lossless double fano cavity)

Figures (spectral detuning):

- Constructed grating trans. spectra (showing the result of varying only the spectral parameters of one grating, λ_0 and λ_1).
- Full range cavity transmission spectra of single + double fano cavities

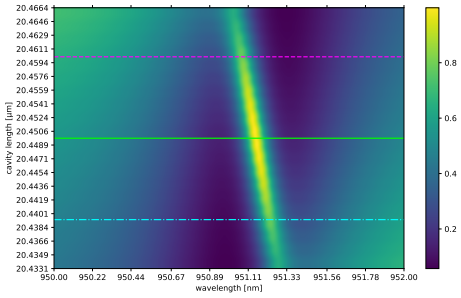

(a) cmap showing transmission as a function of wavelength for cavity lengths ranging $l_g \rightarrow l'_g$.

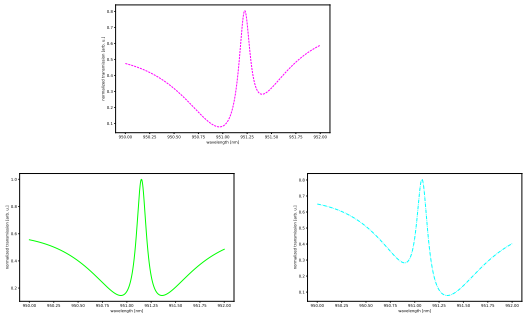

(b) Slices of the cmap showing the optimal length and wavelength of double fano cavity (lossless). HWHMs -> Magenta = 71.3pm, cyan = 71.3pm and lime = 58.6pm.

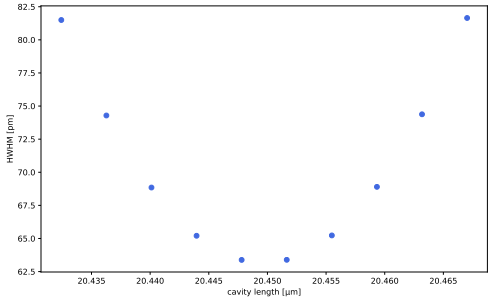

Figure 16: intracavity linewidth as a function of cavity length (same cavity as depicted in cmap above.)

with grating transmission (note: resonance peak is between the trans. minima of the two gratings).

- Cavity trans. spectra for different values of Δ (constant cavity length).
- Linewidth as a function of spectral detuning Δ.

Figures (spacial detuning):

- Cavity trans. spectra for different lengths (small/large detuning comparison).
- Linewidth as a function of cavity length ($l_g \rightarrow l'_g$).

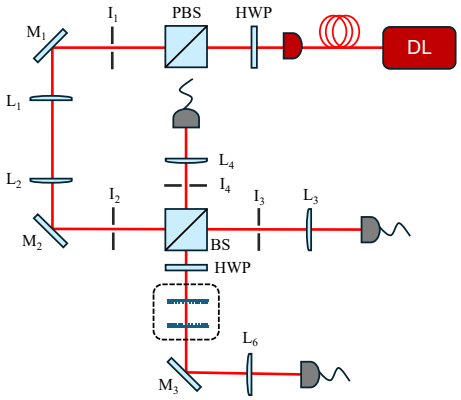

(a) Schematics of the experimental setup for measuringthe transmission through a double fano cavity. The cavity setup shown in (b) is located in position marked by the dotted line.

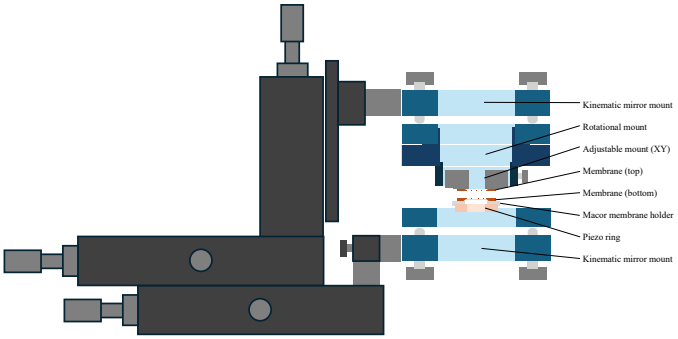

(b) Sketch of the part of the experimental setup containing the optical cavity.

Method

3 Method

3.1 The experimental setup

3.2 Characterization of sub-wavelength grating

Figures:

- Pictures of the membrane before patterning.
- AFM profile of the grating after patterning. (talk about profilometry and the physical parameters of the grating and their meaning for project).
- MAYBE: MIST simulation showing that the model accurately predicts the simulated spectra.

3.2.1 Obtaining normalized transmission/reflection spectra

3.2.2 Adjusting the beam waist - the optical telescope

3.2.3 The alignment procedure

3.2.4 Normalization

3.3 Cavity measurements

3.3.1 Determining the cavity length from the FSR

Figures:

- Linewidth as a function of "time" - to see the reduction of the linewidth as the piezo reaches an equilibrium where any time-dependent drift is reduced.

3.3.2 Normalization

3.3.3 Single fano cavity characterization

3.3.4 Aligning the cavity

Incluce:

- Scan for optimal cavity length
- Measure the spectral linewidth
-

3.3.5 Double fano cavity characterization

3.3.6 Off-resonance Fabry-Perot cavity (alignment technique)

3.3.7 Centering of the top grating (pinhole method)

3.4 Parallelism study (deviation from normal incident)

Results

4 Simulations

4.1 The single Fano cavity

4.2 The double Fano cavity

Figures:

- Simulated spectra of M3 and M5.
- Simulated length scans of M3 and M5.
- M3/M5 cavity trans. spectra (on resonance + full range)

  for lengths: $l_{M3} \rightarrow l_{M5}$

  for length: $l = 1/2 \cdot (l_{M3} + l_{M5})$
- Optimal result comparison with single fano/broadband cavities of similar losses.
- Optimal result comparison with the ideal case from prev. section.
- Simulated linewidth as a function of cavity length (include the same for broadband and single fano cavities).

5 Experimental results

5.1 The single Fano cavity

Figures:

- Single fano cavity transmission as a function of wavelength.
- Short scan of the single fano cavity tranmission, with found linewidth.
- Long scan Fabry-Perot fringes for determining FSR -> cavity length.
- linewidth as a function of cavity length (compare with broadban cavity).

5.2 The double Fano cavity

5.2.1 Realizing the double fano model

Figures:

- Fit of the double fano model (long + short cavity)

5.2.2 Double fano off-resonance Fabry-Perot cavity

Figures:

- Off-resonance double fano transmission as a function of wavelength (show that the off resonance transmission goes close to 100 percent for a well-aligned cavity).

5.2.3 The double fano linewidth

Figures:

- "Semi-short" scan data, fit to the double fano transmission model.
- Short scan data, fit to the Fano function (for measuring linewidth).
- Linewidth as a function of cavity length (compare double fano, single fano and broadband cavitites).

6 Discussion

6.1 Optimal configuration for double fano cavity - spacial limitation for the cavity length

6.2 Spacial drift of the piezo ring

6.3 Noise reduction - coupled/uncoupled mechanical/acoustic vibration (the plexi-glass box)

6.4 Broadening sources (especially for long cavities)

6.5 Improvements to the setup

7 Appendix

- All peaks and fits used for figure 8a.
- All peaks and fits used fir figure **??**.
- The derivation of equation 30
- The derivation of equation 31
- Same derivations for the double fano cavity.

8 References

[1] Marc Eichhorn. *Laser Physics - From Principles to Practical Work in the Lab*. Springer International Publishing Switzerland, 2014.

[2] Frank L. Pedrotti, Leno M. Pedrotti, and Leno S. Pedrotti. *Introduction to Optics, 3rd edition*. Cambridge University Press, 2018.

[3] Shanhui Fan and J. D. Joannopoulos. "Analysis of guided resonances in photonic crystal slabs". In: *Physical Review B* 65 (2002).

[4] U. Fano. "Effects of Configuration Interaction on Intensities and Phase Shifts*". In: *Physical Review* 124.6 (1961).

[5] Ali Akbar Darki. "Nanostructured tramplines for photonics and sensing". PhD thesis. Department of Physics and Astronomy - Aarhus University, 2022.

[6] T. Mitra et al. "Narrow-linewidth Fano microcavities with resonant subwavelength grating mirror". In: *Optics Express* 32.9 (2024).